# The Hydrated Electron at the Surface of Neat Liquid Water Appears To Be Indistinguishable from the Bulk Species

Marc P. Coons, Zhi-Qiang You, and John M. Herbert*

Department of Chemistry and Biochemistry, The Ohio State University, Columbus, Ohio 43210, United States

S *Supporting Information*

ABSTRACT: Experiments have suggested that the aqueous electron, e⁻(aq), may play a significant role in the radiation chemistry of DNA. A recent measurement of the energy (below vacuum level) of the putative "interfacial" hydrated electron at the water/vacuum interface, performed using liquid microjet photoelectron spectroscopy, has been interpreted to suggest that aqueous electrons at the water/biomolecule interface may possess the appropriate energetics to induce DNA strand breaks, whereas e⁻(aq) in bulk water lies too far below the vacuum level to induce such reactions. Other such experiments, however, find no evidence of a long-lived feature at low binding energy. We employ a variety of computational strategies to demonstrate that the energetics of the hydrated electron at the surface of neat liquid water are not significantly different from those of e⁻(aq) in bulk water and as such are incompatible with dissociative electron attachment reactions in DNA. We furthermore suggest that no stable interfacial species may exist at all, consistent with the interpretation of certain surface-sensitive spectroscopy measurements, and that even if a short-lived, metastable species does exist at the vacuum/water interface, it would be extremely difficult to distinguish, experimentally, from e⁻(aq) in bulk water, using either optical absorption or photoelectron spectroscopy.
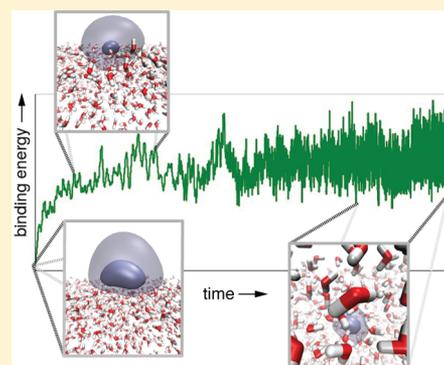
INTRODUCTION

The molecular structure of the air/water interface, including the nature of the dissolved ions that reside there, has attracted attention and controversy for some time.[1−5] An ion that might exist at the interface is the hydrated or aqueous electron, e⁻(aq), a species long known in the radiation chemistry of water.[6−8] The energetics of e⁻(aq) have attracted considerable attention in the context of DNA radiation damage, where it is known that strand breaks are considerably more common in "wet" than in "dry" DNA,[9−11] suggesting that most DNA damage by ionizing radiation is secondary, with the majority of the energy deposited into water rather than absorbed directly by DNA. This raises the question of whether e⁻(aq) might be an intermediate responsible for such damage, but calculations presented here suggest that e⁻(aq), whether at the air/water interface or in bulk water, lies too far below vacuum level to induce DNA strand breaks directly.

Motivated by a controversy regarding surface versus cavity electron-binding motifs in gas-phase $(H_2O)_n^-$ clusters,[12−17] along with the recent development of high-pressure liquid microjet photoelectron spectroscopy,[18,19] several groups have reported photoelectron spectra for liquid-phase e⁻(aq).[20−27] These studies concur that the vertical electron binding energy (VEBE) of e⁻(aq) in bulk water lies in the range 3.3−3.7 eV, with most values around 3.3−3.4 eV,[27] consistent with extrapolations of gas-phase $(H_2O)_n^-$ cluster photoelectron spectra[28] and detailed theoretical calculations.[29]

In one particular microjet experiment, however, a feature at 1.6 eV is observed, with a lifetime ≳100 ps, and is attributed to e⁻(aq) bound at the water/vacuum interface.[20] Attempts by others to replicate this result have found only a transient feature with a lifetime of ∼100 fs,[23,25] even in low kinetic energy experiments that ought to be relatively more sensitive to species solvated near the interface.[25] Nevertheless, there has since arisen much speculation that the putative "interfacial electron" at 1.6 eV might play a role in the radiation chemistry of DNA. Specifically, it is suggested that the much lower VEBE at the interface might provide the proper energetics for dissociative electron attachment to DNA, resulting in single strand breaks.[3,20,30−32]

Although a role in DNA damage for the "pre-solvated electron", a hot precursor to e⁻(aq), has been proposed on the basis of other experiments,[8,33,34] the liquid microjet experiment in ref 20 forms the basis of the first claims that the *equilibrated* species e⁻(aq), as opposed to an excited state, could play a role in radiation damage to DNA. This hypothesis requires that the interfacial species possess an energy ≤2.5 eV below vacuum level,[30,31] in contrast to the consensus value of ≥3.3 eV for the binding energy of thermalized e⁻(aq) in bulk water.[20−29] Here, we investigate the interfacial hydrated electron with detailed theoretical calculations.
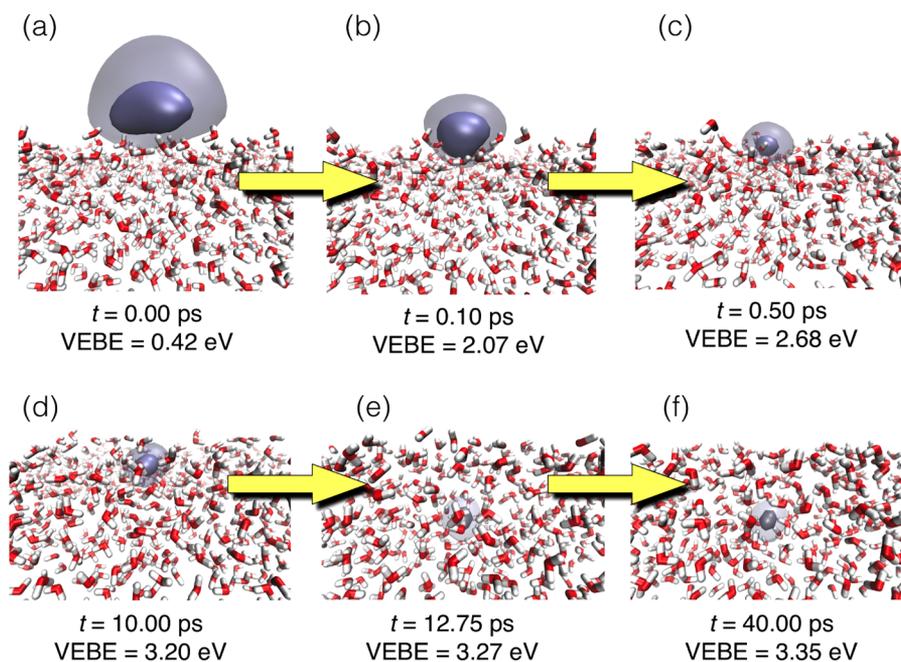
Figure 1. Representative snapshots of a simulation using the mean-field polarization model. In each panel, the opaque blue isocontour of the wave function encapsulates 50% of the one-electron probability distribution $|\psi(\mathbf{r})|^2$, while the lighter, translucent isosurface encloses 95%. At $t = 0$, where the solvent configuration is taken from an equilibrated simulation of neat liquid water, the electron is localized in a surface trap created by dangling O−H moieties, but the degree of localization ($r_g \approx 6.25$ Å) is far less than for $e^-(aq)$ in bulk water. After only 0.1 ps, however, the wave function has contracted to $r_g \approx 3.50$ Å, as seen in (b), while the VEBE has increased by 1.65 eV. By $t = 0.5$ ps, the wave function has contracted to $r_g \approx 2.4$ Å and is comparable in size to the bulk species, yet resides ∼1.0 Å above the Gibbs dividing surface. The size of the wave function has changed little by $t = 10$ ps, but its centroid has moved to 1.50 Å *below* the Gibbs dividing surface and water molecules surround the electron. The VEBE has increased by 0.5 eV relative to (c) and is now comparable to the bulk value. Panel (e) shows a snapshot shortly after the electron internalizes, with its centroid situated 8.74 Å below the Gibbs dividing surface and with a VEBE that is similar to the bulk value and essentially unchanged relative to that in (d). By $t = 40$ ps in (f), the electron centroid has been fluctuating around $d = −8.50$ Å for 28 ps with a VEBE that has fluctuated around the bulk value since $t \approx 10$ ps. An animation of this trajectory is available in the Supporting Information.

■ RESULTS

There is a long history of mixed quantum/classical molecular dynamics (MD) studies of $e^-(aq)$ using one-electron pseudopotential models.[35−37] We report results from simulations employing two variants of such a model: a fully polarizable model that treats electron−water polarization explicitly and self-consistently,[29] and a simpler model[38] wherein polarization is described by a pairwise-additive r^{-4} term in the interaction potential, which is tantamount to a mean-field description of electron−water polarization.[35] Both models successfully reproduce the steady-state absorption spectrum of $e^-(aq)$ as well as the radius of gyration

$$r_g = \langle (\mathbf{r} - \langle \mathbf{r} \rangle) \cdot (\mathbf{r} - \langle \mathbf{r} \rangle) \rangle^{1/2}$$

that is inferred from a moment analysis of this spectrum,[40] and both provide a qualitatively correct value for the rather large diffusion coefficient of $e^-(aq)$.[29,39] The explicit-polarization model also reproduces the aforementioned "consensus" VEBE, along with a variety of ab initio benchmarks for $(H_2O)_n^-$ cluster anions.[29]

Our simulations begin from neat, equilibrated liquid water at $T = 300$ K and $\rho = 0.997$ g/cm^3 in a periodic simulation cell containing 200 water molecules. (Convergence tests with respect to the size of the simulation cell can be found in the Supporting Information.) At time $t = 0$, we introduce the extra electron simply by turning on the electron−water interaction potential, and from this point the energy and forces are obtained from the ground-state eigenvalue of the one-electron

model Hamiltonian. This does not constitute a direct simulation of electron injection into liquid water, except possibly for an electron with zero kinetic energy, but does allow us to examine the interfacial → bulk internalization process because at $t = 0$ the solvent configuration is representative of neat liquid water, and dangling O−H moieties at the water/vacuum interface create a number of shallow potential energy "traps" for the electron to inhabit. As such, the ground-state wave function is fairly localized (at the interface) at $t = 0$, as shown in Figure 1a. Subsequent panels in Figure 1 show how the wave function changes as it evolves in time.

The very early-time dynamics of $e^-(aq)$ at the interface suggest that within even the first 100 fs of solvation dynamics the electron is pulled farther below vacuum level than the reported 1.6 eV for the putative surface-bound electron.[20,30] Although not yet as compact as the equilibrated species, the electron's wave function is certainly localized, whereas previous discussion has assumed that an electron ∼1.6 eV below vacuum level would be delocalized.[11] That assumption is based on a value $V_0 = −1.5$ eV for the band gap of liquid water,[11] meaning that the conduction band sits 1.5 eV below vacuum level. Extrapolations of cluster ion data, however, suggest instead that $V_0 \sim 0$.[41] Moreover, on the surface of amorphous solid water, where the librational dynamics that ultimately solvate the interfacial electron are frozen out, the surface-bound electron is stable for *minutes* and is thought to localize in a Bjerrum defect.[42] The measured VEBE of $e^-(aq)$ on the surface of amorphous solid water is 1.4 eV,[43] consistent with values intermediate between those in Figures 1a and 1b.

Figure 2 depicts the time evolution of the VEBE, the radius of gyration, and the distance d between the centroid of the
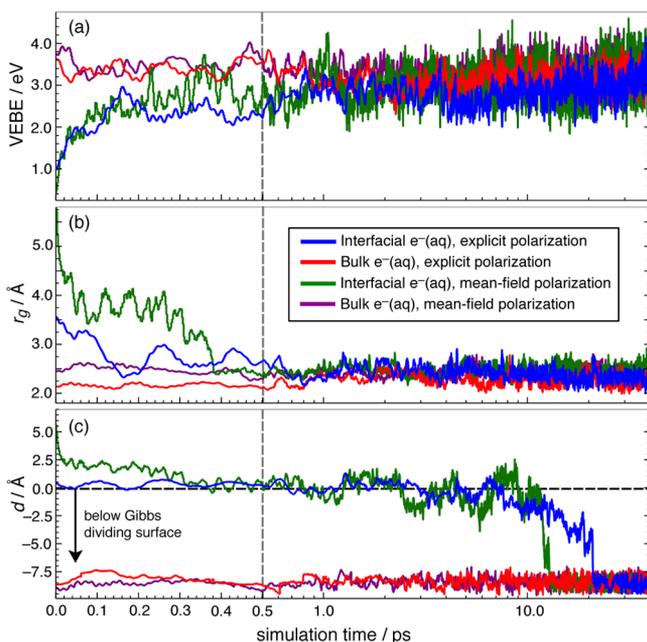

Figure 2. Time evolution of the (a) VEBE, (b) radius of gyration, and (c) distance between the centroid of the e⁻(aq) charge distribution and the Gibbs dividing surface. (The time axis is linear for the first 0.5 ps and then switches to a logarithmic scale.) Data are obtained from quantum/classical MD using two different one-electron models under ambient conditions.

excess electron wave function and the Gibbs dividing surface, which is defined as the locus of points in the z direction for which the solvent density has fallen to half its value in bulk solution, and is used to demarcate the instantaneous liquid/vapor interface. Although initially quite diffuse and weakly bound, the interfacial electron undergoes an ultrafast hydration process that begins to stabilize and localize the diffuse charge within 25 fs via rotation of O−H moieties into the charge cloud. This process increases the VEBE by ∼1 eV. A deuterium isotope effect observed in the early-time signal (35−80 fs) in pump/probe experiments has previously been taken as evidence that librational motion of the waters is responsible for the first stages of electron localization,[44,45] and we observe this directly in our simulations. An additional 1.0−1.5 eV of stabilization occurs in the next 125 fs, and by $t = 0.5−1.0$ ps the VEBE of the interfacial species is essentially indistinguishable from that of e⁻(aq) in bulk water. Concurrently, the size of the interfacial charge collapses from $r_g \approx 6−8$ Å to $r_g \approx 2−3$ Å as shown in Figure 2b. The electron localization time scale that we observe directly in bulk water is consistent with that inferred from time-resolved terahertz spectroscopy.[46]

Twenty trajectories were examined for both the bulk and interfacial electron for each pseudopotential model and for periodic simulation cells containing 200, 300, and 600 water molecules, and in every single case the interfacial electron undergoes a transition into bulk water on a time scale of ∼10−25 ps for the mean-field polarization model and ∼25−35 ps for the explicitly polarizable model (see Figure 2c). This is consistent with previous simulations of relaxation dynamics of e⁻(aq) at the water/vacuum interface at ambient temperature[47] and also with recent work in which the mean-field polarization

model was used to compute the potential of mean force for dragging an electron through the interface.[48,49] In the latter simulations, the free energy profile for moving the electron from the interface to a depth of 9−10 Å is either strictly downhill[48] or else exhibits a barrier to internalization of <2 $k_B T$ (at $T = 300$), depending on how the interface is defined.[49] Electron−water polarization is the only component of the interaction energy that drives the electron inward from the interface,[48,50] and the mean-field r^{-4} polarization potential is known to overestimate the polarization energy relative to explicit, many-body treatments of electron−solvent polarization.[50,51] One might therefore expect that an explicitly polarizable model would afford a slightly longer time scale for internalization as compared to a mean-field polarization model, which is, in fact, what we observe. In any case, the potential of mean force is found to be completely flat for $d < −1$ nm,[48] so the fact that we do not observe bulk-solvated electrons spontaneously return to the interface can be explained based simply on the fact that the volume of phase space consistent with $d < −1$ nm is far greater than that within 1 nm of the interface.

Figure 3 is a scatter plot examining the correlation between the VEBE and the quantities r_g and d. Anticorrelation between
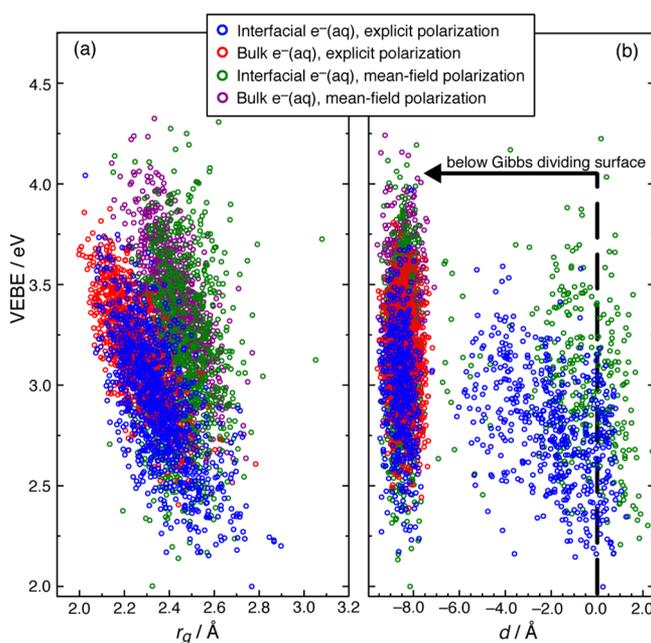

Figure 3. VEBE as a function of the (a) radius of gyration and (b) distance between the electron and the Gibbs dividing surface. The data are taken from the trajectories plotted in Figure 2, sampled every 20 fs.

VEBE and r_g (Figure 3a) is observed for all of the simulations, regardless of initial conditions or which one-electron model is used. This has also been observed in previous simulations of both e⁻(aq)[38,47,53,54] as well as finite $(H_2O)_n^-$ clusters.[17,52] In clusters, the correlation between the VEBE and r_g is observed for both surface-bound isomers (the cluster analogues of the interfacial hydrated electron) as well as "internalized" isomers (analogues of the electron in bulk water). A similar correlation is found between r_g and the electronic absorption maximum in both clusters and for e⁻(aq) in bulk water, although the clusters span a much wider range of r_g values and make it apparent that both the VEBE and the absorption maximum vary with r_g^{-2}, a dependence that can be derived from a particle-in-a-cavity

model for bulk e$^-$(aq) or from a Rydberg atom model for $(H_2O)_n^-$.[17] On the other hand, the VEBE data span a range of ~1 eV (see Figure 3), so while these toy models successfully predict the qualitative r_g^{-2} trend that is somewhat evident in the data in Figure 3a, and more obvious in the cluster data,[17] they cannot quantitatively predict the VEBE. For this, detailed atomistic calculations are required.

In contrast to the correlation with r_g, the VEBE appears to be *uncorrelated* with the distance d from the water/vacuum interface, as has been seen in previous simulations as well.[47,54] Averages for these observables are reported in Table 1 and are essentially unchanged even if half of the trajectories

Table 1. Average Values for Selected Observables from One-Electron Pseudopotential Simulations

polarization method	system	$\langle VEBE \rangle$ (eV)	$\langle r_g \rangle$ (Å)	$\langle d \rangle$ (Å)
explicit	interface^a	3.10	2.27	−2.05
explicit	bulk	3.30	2.21	−8.54
mean-field	interface^a	3.13	2.55	−1.76
mean-field	bulk	3.39	2.43	−8.46

^{a}Averages exclude data points after the electron internalizes.

are discarded. It should be noted that there are important finite-size corrections to the VEBE, which is especially sensitive to long-range Coulomb effects.[29,55] These are addressed in the Supporting Information and with calculations using continuum boundary conditions, as discussed below. What is most important to the present discussion is that the interfacial and bulk VEBEs differ only by about 0.2 eV. Full probability distributions for the bulk and interfacial VEBEs (Figure S3 in the Supporting Information) are consistent with a shift of 0.2 eV, and a broadening of < 0:2 eV, in the VEBE distribution at the interface relative to that in bulk water.

For the bulk species, values of d span a narrow range around −8.5 Å that reflects about half the thickness of the periodic slab used in the simulations. (This is true in larger simulation cells as well; in a 300 H_2O cell with a slab thickness of 20.8 Å, the bulk species fluctuates around $d = -8.9$ Å and in a 600 H_2O cell with a thickness of 26.2 Å it fluctuates around $d = -13.0$ Å, as shown in the Supporting Information.) Evidence of the prompt disappearance of the interfacial species can be seen in Figure 3b, where trajectories initialized at $d = 0$ migrate to $d \approx -8.5$ Å within tens of picoseconds. Once it passes into bulk solution, the electron's VEBE fluctuates between 2.5−3.5 eV, which is roughly the same range observed for the original, interfacial state, for which d ranges from −5 Å to +1 Å. Evidently, the VEBE is controlled by the size of the electron (r_g) but is uncorrelated with its distance from the interface.

This, too, is similar to what is observed in finite clusters.[17] Whereas when the unpaired electron is far from the water cluster, it is dipole-bound and exhibits a VEBE < 0.5 eV, as the centroid of its wave function approaches the cluster surface, the distribution of VEBEs broadens and approaches values similar to the case of a fully solvated electron. Similarly, the present calculations show that even for an interfacial electron that is 1−2 Å above the surface of liquid water, the VEBE spans a range of values comparable to what is observed for e$^-$(aq) in bulk water (see Figure 3b).

Simulations reported here and elsewhere[47,48] suggest that the interfacial species may not be stable beyond a time scale of ~30 ps and, perhaps more importantly, that measurement of the VEBE by photoelectron spectroscopy may be unable to

differentiate between e$^-$(aq) in bulk solution and e$^-$(aq) at the water/vacuum interface. (It is possible that measurement of photoelectron angular distributions might be able to make such a distinction; such a technique has recently been used in an attempt to elucidate electron binding motifs in sodium-doped water clusters.[56]) Photoelectron spectroscopy likely probes the compactness of the solvated electron's spin density, rather than its position relative to the interface, much like terahertz spectroscopy of e$^-$(aq) in bulk water.[46] Recently, we concluded that the steady-state absorption spectrum of e$^-$(aq) that, historically speaking, is the primary observable used to monitor production and annihilation of this species,[57−61] also fails to discriminate e$^-$(aq) in bulk water from that at the interface.[62] As in the photoelectron case, absorption spectroscopy is primarily a probe of the electron's compactness, regardless of binding motif.[17]

Although e$^-$(aq) has been detected in experiments using various surface-sensitive spectroscopies,[63,64] those experiments have been interpreted to imply that that the species responsible for the "interfacial" signal might reside anywhere within the first 1−2 nm of the liquid,[63] and that its lifetime in the vicinity of the interface is < 100 ps.[64] Even at a depth of 1 nm, our calculations suggest that the properties of the nominally "interfacial" electron are actually indistinguishable from those of the equilibrated species in bulk water, owing to the presence of sufficiently many solvation shells to converge r_g. In this interpetation, surface-sensitive spectroscopy simply detects whatever bulk-like electrons happen to diffuse close enough to the surface to break spatial inversion symmetry and thus become observable. This is consistent with an electron attenuation length of ~5 nm at 3 eV of electron kinetic energy,[65] meaning that photoemission from any putative surface-bound species should always be accompanied by a strong signal from the bulk species.[19,27]

To complement the one-electron pseudopotential simulations discussed above, we also computed the VEBE at the level of DFT and MP2 including a quantum-mechanical (QM) description of a significant number of surrounding water molecules. DFT calculations employed a long-range-corrected functional (LRC-μBOP) that has been shown to provide accurate VEBEs for $(H_2O)_n^-$ clusters[66,67] as well as an accurate absorption spectrum for e$^-$(aq) in bulk water.[62] The range-separation parameter, μ, is tuned in a nonempirical way to satisfy the ionization energy (IE) condition[68]

$$\varepsilon_{HOMO}(\mu) = -IE(\mu)$$

and must be adjusted when the size of the QM region changes.[62] (Consult the Supporting Information for details and for tuned values of μ.) MP2 calculations, in contrast, have no such adjustable parameter and have been shown to provide VEBEs within ~0.05 eV of CCSD(T) values for strongly-bound $(H_2O)_n^-$ clusters.[69−71]

The ab initio calculations reported here were performed on snapshots extracted from mixed quantum/classical (QM/MM) simulations of both bulk and interfacial e$^-$(aq),[53,54] which we have previously used to obtain quantitative agreement with the electronic absorption spectrum of the bulk species.[62] From these snapshots, we extract QM regions ranging in radius from 5.5−8.0 Å around the centroid of the spin density ($\rho_\alpha - \rho_\beta$). For the bulk species, this corresponds to ~30 H_2O molecules for the smallest QM regions and ~90 for the largest, whereas for the interfacial species the corresponding numbers are ~20 and ~60 H_2O molecules, respectively.

Table 2. VEBEs[a] (in eV) Computed at the DFT[b]/- and MP2[c]/6-31++G* Levels of Theory Using Nonequilibrium Solvation Models

	bulk e⁻(aq)				interfacial e⁻(aq)	
	PCM		Poisson		Poisson	
QM radius (Å)	DFT	MP2	DFT	MP2	DFT	MP2
5.5	3.52 ± 0.31	3.44 ± 0.35	3.33 ± 0.31	3.18 ± 0.32	3.15 ± 0.41	3.07 ± 0.46
6.0	3.61 ± 0.35	3.42 ± 0.34	3.36 ± 0.32	3.21 ± 0.34	3.18 ± 0.43	3.02 ± 0.40
6.5	3.57 ± 0.38	3.37 ± 0.30	3.40 ± 0.33	3.17 ± 0.34	3.16 ± 0.42	3.06 ± 0.46
7.0	3.53 ± 0.35	3.41 ± 0.31	3.37 ± 0.34	3.19 ± 0.32	3.17 ± 0.41	3.08 ± 0.44
7.5	3.59 ± 0.35	3.42 ± 0.32	3.35 ± 0.31	3.20 ± 0.33	3.14 ± 0.41	3.09 ± 0.43
8.0	3.54 ± 0.32	3.45 ± 0.33	3.39 ± 0.33	3.22 ± 0.35	3.19 ± 0.44	3.10 ± 0.47

[a]Using structures extracted from QM/MM simulations reported in refs 53 and 54. Uncertainties represent one standard deviation. [b]LRC-μBOP with μ tuned individually at each QM size so that $\epsilon_{SOMO} = -IE$. [c]Using the resolution-of-identity (RI) approximation.

To incorporate longer-range solvent effects for e⁻(aq) in bulk water, we employ a nonequilibrium polarizable continuum model (PCM) that uses the solvent's optical dielectric constant to model electronic polarization upon vertical ionization.[72,73] PCM calculations in quantum chemistry usually describe the QM/continuum boundary by means of a union of atom-centered van der Waals spheres,[75] but this makes little sense in the present context given the highly delocalized nature of the solute (an electron), which is not assignable to any particular atom. In addition, with a significant number of solvent molecules considered explicitly within the QM region, the van der Waals cavity construction would allow the interstitial excess electron to inhabit the dielectric medium, to unknown effect. To avoid these problems, we define the boundary between atomistic and continuum regions to consist of a single spherical surface, centered at the centroid of the spin density and whose radius extends 2.75 Å beyond the farthest atom in the QM region. (Consult the Supporting Information for a justification of this choice.)

This spherical-boundary approach is not possible for the interfacial species, where the dielectric medium is spatially anisotropic. In this case, we directly solve Poisson's equation

$$\hat{\nabla} \cdot [\epsilon(\mathbf{r}) \hat{\nabla} \varphi(\mathbf{r})] = -4\pi\rho(\mathbf{r})$$

using an algorithm adapted from ref 76 for a spatially inhomogeneous dielectric function $\epsilon(\mathbf{r})$ that takes the value $\epsilon = 78$ for $d < 0$ and $\epsilon = 1$ for $d > 0$. The QM charge density $\rho(\mathbf{r})$ is discretized onto a three-dimensional grid, and we solve for the electrostatic potential $\varphi(\mathbf{r})$ at each self-consistent field iteration, whereupon the (equilibrium) solvation free energy is

$$G = \frac{1}{2} \int d\mathbf{r} \varphi(\mathbf{r})\rho(\mathbf{r})$$

The converged electrostatic potential $\varphi(\mathbf{r})$ can then be used in the nonequilibrium reaction-field method of refs 72 and 73 in order to compute the change in G upon vertical ionization. This represents a model in which electronic polarization is considered following ionization, but vibrational and orientational polarization is frozen, since the ionization process is vertical in terms of the nuclear coordinates. Additional details of the algorithm can be found in the Supporting Information.

VEBEs computed using these nonequilibrium QM/PCM and QM/Poisson methods are listed in Table 2. For the bulk species, DFT/PCM and MP2/PCM calculations both afford VEBEs of 3.4–3.6 eV, in agreement with the experimental consensus of 3.3–3.7 eV,[20–28] and with prior QM/MM simulations.[53] The computed VEBEs converge rapidly with

respect to the size of the QM region, and even the smallest QM region (comprising approximately two solvation shells around the spin density) affords a VEBE within 0.1 eV of the converged result. This is consistent with observations in previous calculations that the spin density extends outward through two solvation shells, but not three.[29,36,74] Continuum boundary conditions contribute 0.7–1.4 eV to the VEBE (see Table S2 in the Supporting Information) and are, therefore, indispensable for obtaining agreement with experiment. Simulations using the explicitly polarizable one-electron model also suggest a polarization response of ~1.4 eV for vertical ionization of e⁻(aq).[29]

For the bulk species, where the dielectric function is isotropic, solution of Poisson's equation should afford very similar results to the PCM, up to discretization errors and the fact that the PCM provides only an approximate treatment of the volume polarization that arises from the tail of the wave function that penetrates beyond the continuum boundary.[75] Comparing Poisson- and PCM-based VEBEs for the bulk species (Table 2), we find that the former are consistently 0.2 eV smaller but still within the experimentally measured range of bulk e⁻(aq). This favorable comparison validates our implementation of the nonequilibrium Poisson solver that is described in the Supporting Information.

Only the QM/Poisson approach is available for the interfacial species due to the anisotropic nature of the dielectric boundary in this case. The QM/Poisson approach affords an interfacial VEBE that is consistently 0.1–0.2 eV smaller than the bulk value computed with the same algorithm, but this difference is well within statistical fluctuations. Furthermore, the VEBEs computed with the QM/Poisson methodology are in agreement with QM/MM simulations of the interfacial species under periodic boundary conditions,[54] as well as mixed quantum/classical MD simulations of the relaxation dynamics of an excess electron at the vacuum/water interface that employ a one-electron pseudopotential and a much larger periodic simulation cell.[47] Given the quantitative agreement between these various simulation methods, and the fact that they all agree with experimental results for e⁻(aq) in bulk water, our calculations for the interfacial species appear to exclude the possibility of an interfacial solvated electron whose VEBE is significantly smaller than that of e⁻(aq) in bulk water.

■ DISCUSSION

The picture that emerges from this work is one in which librational modes contribute to ultrafast (<1 ps) electron localization, both in bulk water and at the water/vacuum

interface. Simulations indicate that an electron spawned at the interface of neat liquid water is unstable and migrates into bulk water within ~30 ps. Even during the short time that the electron samples a truly interfacial environment, however, we find that its energy (measured relative to vacuum level) is essentially indistinguishable from that of equilibrated aqueous electron in bulk water. Ab initio calculations of the VEBE for the bulk species afford values of 3.4–3.6 eV that agree quantitatively with the experimental consensus of 3.3–3.7 eV but also suggest that the VEBE is not significantly different for the short-lived interfacial species. As such, these calculations lend no support to the idea of an electron at the vacuum/water interface with a VEBE that is significantly smaller than the bulk value.

Our results for both the energy and lifetime of the interfacial species are at odds with a recent experimental report[20] in which a long-lived (≳100 ps) signal at 1.6 eV in a liquid microjet photoelectron spectrum was assigned to an electron bound at the water/vacuum interface. On the basis of electron attachment energies computed for temporary anion resonances in nucleotide monophosphates,[77,78] it was suggested in subsequent review articles[3,30–32] that a hydrated electron situated ≤2.5 eV below vacuum level is in the right range to induce DNA single strand breaks, via dissociative electron attachment. An electron whose VEBE is ~1.6 eV would thus fall into this range, but one whose VEBE is ≥3.3 eV would not.

Recent QM and QM/MM calculations of double-stranded DNA[81] and individual nucleobases[82] in aqueous solution show that the adiabatic electron affinities (EAs) of the DNA bases increase dramatically upon solvation, although the effect saturates after about two solvation shells and values in the range 0.75–1.20 eV are obtained.[82] Both the vertical and adiabatic EAs are relevant in the discussion of electron attachment to DNA, but in aqueous solution one expects the latter to be larger;[20] hence, these values set an upper bound on the VEBE that would make the interfacial hydrated electron relevant to dissociative electron attachment reactions in DNA. Our calculations suggest that the energetics of an electron solvated at the surface of neat liquid water lie well outside of this bound, with both the bulk *and* the interfacial species residing too far below vacuum level. The energetics of this scenario are illustrated schematically in Figure 4.

Notably, the only other microjet experiment to report a feature at 1.6 eV for e⁻(aq) observed this signal to decay in ≲100 fs.[25] That time scale is consistent with the excited-state lifetime of e⁻(aq),[44,45,79,80] and thus it is suggested that the 1.6 eV feature might simply be a short-lived excited state of e⁻(aq).[25] Given that the most probable s → p excitation energy of the equilibrated species in bulk water is 1.7 eV,[28] a VEBE of 1.6 eV for an excited state is consistent with a ground-state VEBE of 3.3 eV.

Results presented here appear to close the door on the notion that an electron at the surface of neat liquid water is responsible for the 1.6 eV binding energy that is reported in ref 20, but leave open the question of the chemical identity of the species responsible for this feature. Its energetics are uncannily similar to the s → p excited state of e⁻(aq),[62] whether in bulk water or at the interface, but the ≳100 ps lifetime for this signal that is reported in ref 20 is inconsistent with the <1 ps excited-state lifetime that is reported elsewhere.[44,45,79,80] There exists speculation that this signal might be attributable to a Rydberg anion supported by H_3O^+ at the interface, where the hydronium ion might occur naturally or might have been
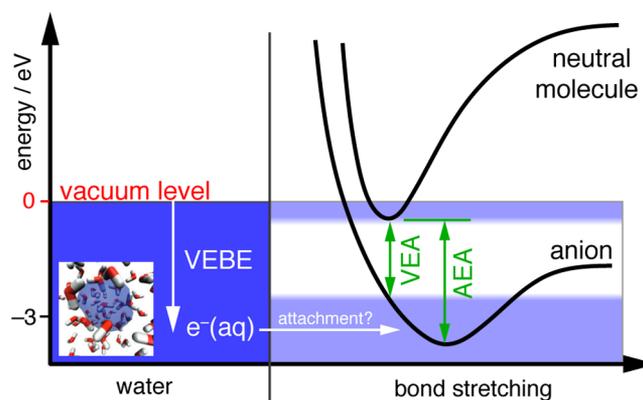

Figure 4. Hypothetical potential energy curves for dissociative electron attachment via e⁻(aq). The molecular anion formed by electron attachment is stabilized by aqueous solvation, relative to its neutral parent molecule. The white band on the right illustrates the window between the vertical electron affinity (VEA) and the adiabatic electron affinity (AEA) in which electron attachment is energetically feasible; the left part of the diagram suggests that the equilibrated species e⁻(aq) lies too far below vacuum level for this process to occur. Adapted from ref 20; copyright 2010 Nature Publishing Group.

created photochemically as a side product of two-photon ionization of water.[32] Such speculation may suggest new calculations aimed to interpret experimental measurements that seek to understand the nature of the air/water interface.

■ ASSOCIATED CONTENT

Ⓢ Supporting Information
The Supporting Information is available free of charge on the ACS Publications website at DOI: 10.1021/jacs.6b06715.

> Additional details about the calculations, including convergence tests for the trajectory simulations, trajectory animations, range separation parameters for the DFT calculations, continuum solvation energies, and details of the algorithm used to solve Poisson's equation (PDF)
> Simulation with N = 200 water molecules (AVI)
> Simulation with N = 600 water molecules (AVI)

■ AUTHOR INFORMATION

Corresponding Author
*herbert@chemistry.ohio-state.edu

Notes
The authors declare no competing financial interest.

■ ACKNOWLEDGMENTS

■ REFERENCES

(1) Jungwirth, P.; Tobias, D. J. *Chem. Rev.* **2006**, *106*, 1259–1281.
(2) Chaplin, M. *Water* **2009**, *1*, 1–28.
(3) Abel, B. *Annu. Rev. Phys. Chem.* **2013**, *64*, 533–552.
(4) Levin, Y.; dos Santos, A. P. *J. Phys.: Condens. Matter* **2014**, *26*, 203101–11.
(5) Bai, C.; Herzfeld, J. *ACS Cent. Sci.* **2016**, *2*, 225–231.
(6) Hart, E. J.; Anbar, M. *The Hydrated Electron*; Wiley-Interscience, 1970.

(7) Buxton, G. V.; Greenstock, C. L.; Helman, W. P.; Ross, A. B.; Tsang, W. *J. Phys. Chem. Ref. Data* **1988**, *17*, 513−886.

(8) Alizadeh, E.; Sanche, L. *Chem. Rev.* **2012**, *112*, 5578−5602.

(9) Ito, T.; Baker, S. C.; Stickley, C. D.; Peak, J. G.; Peak, M. *Int. J. Radiat. Biol.* **1993**, *63*, 289−296.

(10) Falcone, J. M.; Becker, D.; Sevilla, M. D.; Swarts, S. G. *Radiat. Phys. Chem.* **2005**, *72*, 257−264.

(11) Alizadeh, E.; Sanz, A. G.; García, G.; Sanche, L. *J. Phys. Chem. Lett.* **2013**, *4*, 820−825.

(12) Verlet, J. R. R.; Bragg, A. E.; Kammrath, A.; Cheshnovsky, O.; Neumark, D. M. *Science* **2005**, *307*, 93−96.

(13) Turi, L.; Sheu, W.-S.; Rossky, P. J. *Science* **2005**, *309*, 914−917.

(14) Verlet, J. R. R.; Bragg, A. E.; Kammrath, A.; Cheshnovsky, O.; Neumark, D. M. *Science* **2005**, *310*, 1769−1769.

(15) Turi, L.; Sheu, W.-S.; Rossky, P. J. *Science* **2005**, *310*, 1769−1769.

(16) Ma, L.; Majer, K.; Chirot, F.; von Issendorff, B. *J. Chem. Phys.* **2009**, *131*, 144303−6.

(17) Jacobson, L. D.; Herbert, J. M. *J. Am. Chem. Soc.* **2011**, *133*, 19889−19899.

(18) Winter, B.; Faubel, M. *Chem. Rev.* **2006**, *106*, 1176−1211.

(19) Seidel, R.; Thürmer, S.; Winter, B. *J. Phys. Chem. Lett.* **2011**, *2*, 633−641.

(20) Siefermann, K. R.; Liu, Y.; Lugovoy, E.; Link, O.; Faubel, M.; Buck, U.; Winter, B.; Abel, B. *Nat. Chem.* **2010**, *2*, 274−279.

(21) Tang, Y.; Shen, H.; Sekiguchi, K.; Kurahashi, N.; Mizuno, T.; Suzuki, Y. I.; Suzuki, T. *Phys. Chem. Chem. Phys.* **2010**, *12*, 3653−3655.

(22) Shreve, A. T.; Yen, T. A.; Neumark, D. M. *Chem. Phys. Lett.* **2010**, *493*, 216−219.

(23) Lübcke, A.; Buchner, F.; Heine, N.; Hertel, I. V.; Schultz, T. *Phys. Chem. Chem. Phys.* **2010**, *12*, 14629−14634.

(24) Horio, T.; Shen, H.; Adachi, S.; Suzuki, T. *Chem. Phys. Lett.* **2012**, *535*, 12−16.

(25) Buchner, F.; Schultz, T.; Lübcke, A. *Phys. Chem. Chem. Phys.* **2012**, *14*, 5837−5842.

(26) Yamamoto, Y.; Suzuki, Y.-I.; Tomasello, G.; Horio, T.; Karashima, S.; Mitríc, R.; Suzuki, T. *Phys. Rev. Lett.* **2014**, *112*, 187603−5.

(27) Yamamoto, Y.; Karashima, S.; Adachi, S.; Suzuki, T. *J. Phys. Chem. A* **2016**, *120*, 1153−1159.

(28) Coe, J. V.; Williams, S. M.; Bowen, K. H. *Int. Rev. Phys. Chem.* **2008**, *27*, 27−51.

(29) Jacobson, L. D.; Herbert, J. M. *J. Chem. Phys.* **2010**, *133*, 154106−19.

(30) Siefermann, K. R.; Abel, B. *Angew. Chem., Int. Ed.* **2011**, *50*, 5264−5272.

(31) Abel, B.; Buck, U.; Sobolewski, A. L.; Domcke, W. *Phys. Chem. Chem. Phys.* **2012**, *14*, 22−34.

(32) Faubel, M.; Siefermann, K. R.; Liu, Y.; Abel, B. *Acc. Chem. Res.* **2012**, *45*, 120−130.

(33) Wang, C.-R.; Nguyen, J.; Lu, Q.-B. *J. Am. Chem. Soc.* **2009**, *131*, 11320−11322.

(34) Lu, Q.-B. *Mutat. Res., Rev. Mutat. Res.* **2010**, *704*, 190−199.

(35) Sommerfeld, T.; DeFusco, A.; Jordan, K. D. *J. Phys. Chem. A* **2008**, *112*, 11021−11035.

(36) Herbert, J. M.; Jacobson, L. D. *Int. Rev. Phys. Chem.* **2011**, *30*, 1−48.

(37) Turi, L.; Rossky, P. J. *Chem. Rev.* **2012**, *112*, 5641−5674.

(38) Turi, L.; Borgis, D. *J. Chem. Phys.* **2002**, *117*, 6186−6195.

(39) Herbert, J. M.; Jacobson, L. D. *J. Phys. Chem. A* **2011**, *115*, 14470−14483.

(40) Carmichael, I. *Chem. Phys. Lett.* **1978**, *56*, 339−342.

(41) Coe, J. V. *Int. Rev. Phys. Chem.* **2001**, *20*, 33−58.

(42) Bovensiepen, U.; Gahl, C.; Stähler, J.; Bockstedte, M.; Meyer, M.; Baletto, F.; Scandolo, S.; Zhu, X.-Y.; Rubio, A.; Wolf, M. *J. Phys. Chem. C* **2009**, *113*, 979−988.

(43) Stähler, J.; Deinert, J.-C.; Wegkamp, D.; Hagen, S.; Wolf, M. *J. Am. Chem. Soc.* **2015**, *137*, 3520−3524.

(44) Silva, C.; Walhout, P. K.; Yokoyama, K.; Barbara, P. F. *Phys. Rev. Lett.* **1998**, *80*, 1086−1089.

(45) Yokoyama, K.; Silva, C.; Son, D. H.; Walhout, P. K.; Barbara, P. F. *J. Phys. Chem. A* **1998**, *102*, 6957−6966.

(46) Savolainen, J.; Uhlig, F.; Ahmed, S.; Hamm, P.; Jungwirth, P. *Nat. Chem.* **2014**, *6*, 697−701.

(47) Madarász, Á; Rossky, P. J.; Turi, L. *J. Chem. Phys.* **2007**, *126*, 234707−11.

(48) Glover, W.; Casey, J. R.; Schwartz, B. J. *J. Chem. Theory Comput.* **2014**, *10*, 4661−4671.

(49) Casey, J. R.; Schwartz, B. J.; Glover, W. J. *J. Phys. Chem. Lett.* **2016**, *7*, 3192−3198.

(50) Stampfli, P. *Phys. Rep.* **1995**, *255*, 1−77.

(51) Voora, V. K.; Ding, J.; Sommerfeld, T.; Jordan, K. D. *J. Phys. Chem. B* **2013**, *117*, 4365−4370.

(52) Turi, L.; Madarász, Á; Rossky, P. J. *J. Chem. Phys.* **2006**, *125*, 014308−7.

(53) Uhlig, F.; Marsalek, O.; Jungwirth, P. *J. Phys. Chem. Lett.* **2012**, *3*, 3071−3075.

(54) Uhlig, F.; Marsalek, O.; Jungwirth, P. *J. Phys. Chem. Lett.* **2013**, *4*, 338−343.

(55) Turi, L. *J. Chem. Phys.* **2016**, *144*, 154311−9.

(56) West, A. H. C.; Yoder, B. L.; Luckhaus, D.; Saak, C.-M.; Doppelbauer, M.; Signorell, R. *J. Phys. Chem. Lett.* **2015**, *6*, 1487−1492.

(57) Jou, F.-Y.; Freeman, G. R. *J. Phys. Chem.* **1977**, *81*, 909−915.

(58) Jou, F.-Y.; Freeman, G. R. *J. Phys. Chem.* **1979**, *83*, 2383−2387.

(59) Tuttle, T. R., Jr.; Golden, S. *J. Phys. Chem.* **1980**, *84*, 2457−2458.

(60) Tuttle, T. R., Jr.; Golden, S. *J. Chem. Soc., Faraday Trans. 2* **1981**, *77*, 873−888.

(61) Tuttle, T. R.; Golden, S.; Lwenje, S.; Stupak, C. M. *J. Phys. Chem.* **1984**, *88*, 3811−3818.

(62) Uhlig, F.; Herbert, J. M.; Coons, M. P.; Jungwirth, P. *J. Phys. Chem. A* **2014**, *118*, 7507−7515.

(63) Sagar, D. M.; Bain, C. D.; Verlet, J. R. R. *J. Am. Chem. Soc.* **2010**, *132*, 6917−6919.

(64) Tuttle, T. R.; Golden, S.; Lwenje, S.; Stupak, C. M. *J. Phys. Chem.* **1984**, *88*, 3811−3818.

(65) Signorell, R.; Goldmann, M.; Yoder, B. L.; Bodi, A.; Chasovskikh, E.; Lang, L.; Luckhaus, D. *Chem. Phys. Lett.* **2016**, *658*, 1−6.

(66) Yagi, K.; Okano, Y.; Sato, T.; Kawashima, Y.; Tsuneda, T.; Hirao, K. *J. Phys. Chem. A* **2008**, *112*, 9845−9853.

(67) Jacobson, L. D.; Williams, C. F.; Herbert, J. M. *J. Chem. Phys.* **2009**, *130*, 124115−18.

(68) Baer, R.; Livshits, E.; Salzner, U. *Annu. Rev. Phys. Chem.* **2010**, *61*, 85−109.

(69) Herbert, J. M.; Head-Gordon, M. *J. Phys. Chem. A* **2005**, *109*, 5217−5229.

(70) Herbert, J. M.; Head-Gordon, M. *Phys. Chem. Chem. Phys.* **2006**, *8*, 68−78.

(71) Herbert, J. M. The quantum chemistry of loosely bound electrons. In *Reviews in Computational Chemistry*; Parill, A. L., Lipkowitz, K., Eds.; Wiley-VCH, 2016; Vol. *28*, Chapter 8, pp 391−517.

(72) Mewes, J.-M.; You, Z.-Q.; Wormit, M.; Kriesche, T.; Herbert, J. M.; Dreuw, A. *J. Phys. Chem. A* **2015**, *119*, 5446−5464.

(73) You, Z.-Q.; Mewes, J.-M.; Dreuw, A.; Herbert, J. M. *J. Chem. Phys.* **2015**, *143*, 204104−14.

(74) Williams, C. F.; Herbert, J. M. *J. Phys. Chem. A* **2008**, *112*, 6171−6178.

(75) Herbert, J. M.; Lange, A. W. Polarizable continuum models for (bio)molecular electrostatics: Basic theory and recent developments for macromolecules and simulations. In *Many-Body Effects and Electrostatics in Biomolecules*; Cui, Q., Ren, P., Meuwly, M., Eds.; Pan Stanford, 2016; Chapter 11, pp 363−416.

(76) Fisicaro, G.; Genovese, L.; Andreussi, O.; Marzari, N.; Goedecker, S. *J. Chem. Phys.* **2016**, *144*, 014103−12.

(77) Gu, J.; Xie, Y.; Schaefer, H. F., III *ChemPhysChem* **2006**, *7*, 1885−1887.

(78) Gu, J.; Xie, Y.; Schaefer, H. F., III *J. Am. Chem. Soc.* **2006**, *128*, 1250−1252.

(79) Bragg, A. E.; Verlet, J. R. R.; Kammrath, A.; Cheshnovsky, O.; Neumark, D. M. *Science* **2004**, *306*, 669−671.

(80) Bragg, A. E.; Verlet, J. R. R.; Kammrath, A.; Cheshnovsky, O.; Neumark, D. M. *J. Am. Chem. Soc.* **2005**, *127*, 15283−15295.

(81) Hübsch, A.; Endres, R. G.; Cox, D. L.; Singh, R. R. P. *Phys. Rev. Lett.* **2005**, *94*, 178102-1.

(82) Smyth, M.; Kohanoff, J. *Phys. Rev. Lett.* **2011**, *106*, 238108-1.

(83) Ohio Supercomputer Center. http://osc.edu/ark:/19495/f5s1ph73.